Dual receptive fields underlying target and motion sensitivity in looming sensitive descending neurons

Sarah Nicholas[1], Yuri Ogawa[1] and Karin Nordström[1,2]*

[1]Flinders Health and Medical Research Institute, Flinders University, GPO Box 2100, Adelaide, SA, 5001, Australia; [2]Department of Medical Cell Biology, Uppsala University, 75123 Uppsala, Sweden

*email: karin.nordstrom@flinders.edu.au

ORCIDs

Sarah Nicholas: 0000-0002-5555-9421

Yuri Ogawa: 0000-0002-9708-7063

Karin Nordström: 0000-0002-6020-6348

Keywords

Target motion, insect vision, motion vision, hoverfly, descending neuron, wide-field motion

Abstract

When an animal is pursuing a target, such as a bird pursuing prey, the retinal projection of the target is initially very small. However, prior to successful capture, as the pursuer nears the target, the image becomes a rapidly expanding object. This suggests that different neural pathways underlie these two behavioural stages: one tuned to small retinal objects, and one to larger, looming stimuli. Indeed, in zebrafish, two different optic brain regions support the initial visualization of prey and the final stages of prey capture. The pursuit of small targets is not limited to vertebrates, with many invertebrates also utilizing these capabilities for prey capture, territorial defences, or courtship. Male *Eristalis tenax* hoverflies, which are highly territorial, have target tuned neurons that likely underlie the initial stages of target detection and pursuit. However, the underlying neuronal control of the final stages of prey capture is currently unknown. We here show a class of descending neurons with dual sensitivity, separated into two distinct receptive fields. The dorsal receptive field shows sensitivity to small targets whereas the ventral receptive field responds to larger objects and looming stimuli. We show that the two receptive fields have different pre-synaptic input, where the inputs are not linearly summed. This novel and unique arrangement could thus support the different stages of target pursuit behavior, where targets are initially detected in the dorsal receptive field, whilst the ventral receptive field is used during the final stages of pursuit and eventual capture.

Introduction

The ability to respond quickly to visual stimuli is vital for the survival of many animals. Indeed, visual input may be used for a variety of tasks, from navigating and avoiding obstacles, choosing a suitable surface to rest upon, and also for detecting predators or prey. For example, many predatory insects rely on vision to identify suitable prey, which they then pursue with astonishing precision and accuracy (e.g. 1, 2, 3). Some non-predatory insects also have superb target detecting capabilities, which they may use to defend their territory against intruders or to pursue potential mates for courtship (4, 5).

Blowflies, houseflies and hoverflies pursue not only conspecifics in the field, but also artificial targets in man-made arenas (6-8), thus allowing more precise quantification of the target image during pursuit. Such experiments have shown that male *Eristalis tenax* hoverflies initiate pursuit of targets that subtend about 0.9 – 1.7° moving at 20 – 170°/s (25th – 75th percentiles) (7). Small target motion detector (STMD) neurons in the hoverfly optic lobe, and their presumed post-synaptic targets, the target selective descending neurons (TSDNs), have size and velocity tuning properties that match the target image at the start of the pursuit, suggesting that they could support these behaviours (9, 10). However, later during pursuit, as the hoverfly closes in on the target, its projected retinal image becomes larger, and eventually becomes a looming stimulus (7). This suggests that another subset of neurons, tuned to larger and looming objects, may be recruited in the later stages of target pursuit (see e.g. Discussion in Ref. 11). Indeed, in zebrafish larvae separate neuronal pathways control the initial detection of prey and initiation of pursuit, versus subsequent prey tracking and capture manoeuvres (12).

Neurons that respond well to rapidly looming stimuli exist in a range of species and visual structures, including the cat superior colliculus (13), the bullfrog optic tectum (14), and in

zebrafish retinal ganglion cells (15). In insects, there are looming neurons in the optic lobes as well as in the descending pathways. For example, the locust LGMD/DCMD system (16), the *Drosophila* Foma-1 neurons (17) and descending giant fiber (18), are likely used for rapid avoidance of bird predators. Interestingly, many of these looming neurons also respond strongly to small moving targets. For example, the locust LGMD/DCMD pathway was originally thought to play a role in object tracking (19), and several looming sensitive neurons in the locust central complex also respond to small moving targets (20). Conversely, some dragonfly target selective descending neurons (TSDNs) respond to both targets and to looming stimuli (21)(22).

Historically, looming neurons have been studied in the context of predator avoidance (e.g. 16, 18, 23). However, there is emerging evidence that such neurons also play a key role in pursuit behaviours. For example, zebrafish larvae usually detect prey in the lateral visual field, but then centre the prey image (24, 25), where it becomes a rapidly expanding stimulus. This last part of the pursuit is likely controlled by loom sensitive, non-directional, inter-ocular neurons in the anterior tectum (12, 26). Similarly, silencing *Drosophila* Foma-1 neurons does not only affect the escape response (17), but also the ability of male flies to follow females during courtship (27).

Taken together, this suggests that some neurons classically defined as either target or looming selective (21, 28) respond to both, and this dual sensitivity could serve a useful role in pursuit behaviours. Like locusts (28) and dragonflies (21), hoverflies have descending neurons that respond to both looming stimuli and to small moving targets (9). We here investigate this dual sensitivity in detail and find these neurons have two distinct receptive fields, one dorsal that responds selectively to the motion of small targets, and one ventral that responds to larger objects, including sinusoidal gratings and high-contrast edges. We show

that when the centre of the ventral grating receptive field is to the right of the visual midline, it prefers motion to the right, and vice versa. However, there is no correlation between the preferred direction of the dorsal target receptive field and the ventral grating receptive field. We also show that the two receptive fields receive separate input, from the pre-synaptic target pathway and the pre-synaptic widefield motion pathway, respectively. However, when receiving dual input, these are not linearly summed. We hypothesize that the unique response characteristics of these neurons make them highly suitable for the control of different stages of target pursuit, with distinct receptive fields sensitive to both small targets and larger rapidly looming objects.

Materials and Methods

Electrophysiology

We recorded from 102 looming sensitive descending neurons (9) in 99 male *Eristalis tenax* hoverflies, reared and maintained in-house as described previously (29). At experimental time the hoverfly was immobilized ventral side up, using a beeswax and resin mixture, before an opening was made in the thoracic cavity. A small silver hook was used to elevate and support the cervical connective and a silver wire inside the opening served as a reference electrode.

Recordings were made from the cervical connective using a sharp polyimide-insulated tungsten microelectrode (2 MOhm, Microprobes, Gaithersburg, USA). Signals were amplified at 100x gain and filtered through a 10 – 3000 Hz bandwidth filter using a DAM50 differential amplifier (World Precision Instruments, Sarasota, USA), with 50 Hz noise removed with a HumBug (Quest Scientific, North Vancouver, Canada). The data were digitized via a Powerlab 4/30 and recorded at 40 kHz with LabChart 7 Pro software

(ADInstruments, Sydney, Australia). Single units were discriminated by amplitude and half-width using Spike Histogram software (ADInstruments).

Visual stimuli

Hoverflies were positioned perpendicular to and 6.5 cm from the middle of a linearized Asus LCD screen (Asus, Taipei, Taiwan) with a mean illuminance of 200 Lux, a refresh rate of 165 Hz and a spatial resolution of 2,560 × 1,440 pixels (59.5 x 33.5 cm), giving a projected screen size of 155 × 138°. Visual stimuli were displayed using custom software written in Matlab (R2019b, Mathworks) using the Psychophysics toolbox (30, 31). The stimuli were not perspective corrected. When values are given in degrees, this corresponds to the retinal size in the centre of the visual field. Velocities are given in pixels/s.

Potential looming sensitive descending neurons were initially identified based on their response to a small, black, moving target (left, Fig. 1, and see Ref. 9). Those neurons that also responded strongly to a looming stimulus compared to an appearance control (9) were kept for further analysis. The looming stimulus was a black circle on a white background, expanding over 1 s from 1° diameter to 117° (right, Fig. 1), with a 10 ms rate of expansion (32), also referred to as $l/|v|$. The appearance control was a black circle with 117° diameter that appeared and remained on the screen for 1 s.

We mapped the target receptive field (9) of each neuron by scanning a target horizontally and vertically at 20 evenly spaced elevations and azimuths (9) to create a 20 x 20 grid (Fig. S1A). The 15 x 15 pixel (3 x 3°) black, square target moved at a velocity of 900 pixels/s. There was a minimum 0.5 s interval between each stimulation.

We mapped the grating receptive field (9) using local sinusoidal gratings (400 x 400 pixels, 71 x 71° in the visual field centre, Fig. S1B) where the internal pattern moved in a series of 8

different directions presented in a pseudorandom order for 0.36 s each. The gratings had a wavelength of 75 pixels (13° for the central patch, 0.08 cpd) and drifted at 5 Hz. The local gratings were placed in an overlapping tiling fashion so that 8 x 6 (width x height) squares covered the majority of the screen (Fig. S1B). There was a minimum 1 s interval between each stimulation.

To map the leading-edge receptive field, we scanned the entire height or width of the screen with an OFF-contrast edge moving left, right, down or up, at 900 pixels/s (Fig. S3A-D).

For size tuning experiments a bar drifted at 900 pixels/s, in the preferred direction of each neuron's target receptive field. The bar drifted either horizontally or vertically through the centre of the target or grating receptive field, as specified. The bar side parallel to the direction of travel was maintained at a fixed size of 15 pixels, i.e. 3°, whilst the perpendicular side varied from 0.2° to 155° (1 pixel to the full height of the screen). When presented simultaneously with a small target, the bar moved in the preferred horizontal direction through the grating receptive field only. In this case the bar height was varied between 5.7° and 106° (28 to 749 pixels), whilst a fixed size 3 x 3° target moved through the target receptive field.

To determine the input mechanism of each receptive field, an OFF edge, an ON edge and a discrete bar, with a width of 15 pixels (3°) drifted horizontally at 900 pixels/s in each neuron's preferred direction, across the entire width of the screen. The height of these objects was 3° (15 pixels) when drifted through the target receptive field, 84° (500 pixels) when drifted through the grating receptive field, or the height of the screen (138°) to cover both receptive fields.

153 All stimuli were presented in a random order, with the exception of the receptive field
154 stimuli, which were presented in a pseudo-random order.

155 ***Data analysis and statistics***

156 All data analysis was performed in Matlab and GraphPad Prism 9.3.1 (GraphPad Software,
157 USA). The sample size, statistical test and P-values are indicated in each figure legend, where
158 *n* refers to the number of repetitions within one neuron and *N* to the number of neurons.
159 Neurons were initially identified based on the response to a small target, with data from all
160 neurons that passed our definition of a looming neuron (Ref. 9, and see above) included in
161 the analysis.

162 For target receptive field mapping we used the resulting 20 x 20 grid (Fig. S1A) to calculate
163 the local preferred direction and local motion sensitivity (Fig. S1C), assuming a neural delay
164 of 20 ms. We calculated the local average response to the four directions of motion (dotted
165 line, Fig. S1C) after subtracting the spontaneous rate, calculated in the 485 ms prior to
166 stimulus presentation. We interpolated this to 100 x 100 grid to generate receptive field maps
167 (Fig. S1E) using Matlab's *contour* function. We defined the centre of the receptive field (Fig.
168 S1E) as the centre of the 50% contour line using Matlab's *centroid* function. We fitted a
169 cosine function (9) to the response to the four directions of motion (10) and extracted its
170 preferred direction and amplitude (Fig. S1C). We calculated the preferred direction for each
171 neuron by averaging the local preferred directions from the locations where the local motion
172 sensitivity was above 50% of the maximum (blue, Fig. S1G).

173 For the grating receptive fields we used the resulting 8 x 6 grid (Fig. S1B) to quantify the
174 local mean response for each direction of motion, after removing the first 100 ms of the
175 response, to avoid any initial onset transients (33, 34). We calculated the local mean response
176 (dotted line, Fig. S1D) after subtracting the spontaneous rate, calculated for 800 ms preceding

stimulus presentation. We spatially interpolated this 10 times and calculated the centre from the 50% contour line (Fig. S1F). For each spatial location we fitted a cosine function (Fig. S1D) to the response to get the local preferred direction and local motion sensitivity (9). We calculated the overall direction selectivity using the top 50% of the local preferred directions (red, Fig. S1H).

We calculated the horizontal and vertical distance between the receptive field centres and the midline and equator. The distance between the two receptive field centres was calculated using the Euclidean distance.

For leading-edge receptive field mapping we first quantified the spike histogram for each neuron, after smoothing the response with a 100 ms square-wave filter with 40 kHz resolution (Fig. S3A-D). We identified the maximum response to any direction of motion (purple, Fig. S3D). 50% maximum response was used as a threshold to determine the limits of the leading-edge receptive field (cyan, Fig. S3A, C, D). If a neuron's response did not reach threshold to one direction of motion (Fig. S3B), the opposite direction of motion determined the receptive field outlines. If a neuron responded to both directions of motion (e.g. up and down) the outer thresholds were used to delineate the receptive field (Fig. S3E). From the resulting rectangular receptive field, we determined the centre, and the proximity to the target and the grating receptive fields respectively (Fig. S3F), using the following proximity index:

$$(d1 - d2) / (d1 + d2)$$

where *d1* is the Euclidean distance between the leading edge and the target receptive field centres, and *d2* the Euclidean distance between the leading edge and the grating receptive field centres (Fig. 4B). Thus, if the leading-edge receptive field centre was closer to the

200 grating receptive field centre, the proximity index was positive, but if it was closer to the
201 target receptive field centre the proximity index was negative.

202 For all stimuli other than receptive field mapping, quantification of responses was done by
203 averaging the spike rate within a 0.56 s analysis window centred on each neuron's target or
204 grating receptive field centre, as specified.

205 Results

206 *Looming neurons have dorsal target receptive fields and ventral grating receptive fields*

207 We recorded from 102 looming sensitive descending neurons in male *Eristalis tenax*
208 hoverflies. The neurons described here responded both to small target motion (left, Fig. 1)
209 and to looming stimuli (right, Fig. 1). The response to a looming stimulus (right, Fig. 1B, D)
210 started well before the stimulus reached its full size (right, Fig. 1C), and was much stronger
211 than the response to an appearance control (not shown, but see Ref. 9).

212 To investigate this dual sensitivity (Fig. 1) in more detail, we mapped the receptive fields
213 using two different methods. For this purpose we either scanned the visual monitor with a
214 small, black target (10) moving in four different directions (Fig. S1A, C), or we used a local
215 sinusoidal grating (Fig. S1B, D) where the internal pattern drifted in eight different directions
216 (9). The data from an example neuron shows two distinct receptive fields, with a dorsal target
217 receptive field (blue, Fig. 2A, S1E), and a ventral grating receptive field (red, Fig. 2B, S1F).

218 We used the 50% response contours to define the two receptive field centres (blue and red
219 circle, Fig. 2A, S1E, F). Across the 102 neurons, the target receptive fields cluster above the
220 visual equator (blue, Fig. 2B), whereas the grating receptive field centres cluster below the
221 equator (red, Fig. 2B), even if there are some exceptions (see also Fig. S2). We quantified the

222 vertical distance between each receptive field centre and the visual equator (41° and -34° in
223 the example neuron, Fig. 2A), and found a bimodal distribution with target receptive field
224 centres peaking 30-40° dorsal and grating receptive field centres peaking 30-40° ventral (Fig.
225 2B, C).

226 We next quantified the horizontal distance between each receptive field centre and the visual
227 midline (14° and 18° in the example neuron, Fig. 2A). Across neurons we found a bimodal
228 distribution with a gap along the visual midline and a peak distribution about 20° either side
229 of the visual midline (Fig. 2B, D). There was no clear lateral distribution difference between
230 the two receptive field types.

231 We noted that the target receptive field was often in the dorsal visual field, but that there
232 were some exceptions (Fig. 2A-C, S2). We next investigated if the target receptive field was
233 always dorsal to the grating receptive field and determined the Euclidean distance between
234 the two receptive field centres (black line, 69°, Fig. 2A). Across neurons we found that the
235 target receptive field was indeed most often dorsal to the grating receptive field (grey, Fig.
236 2E), and that the distance could be quite large. When the grating receptive field was more
237 dorsal, the two receptive field centres tended to be closer to each other (black, Fig. 2E).

238 *The grating receptive field is sensitive to motion away from the midline*

239 We next determined the local motion sensitivity and average preferred direction of each
240 neuron's target and grating receptive field (coloured arrows, Fig. S1G, H, S2). In the example
241 neuron, the preferred direction of the target receptive field is up and toward the visual
242 midline (blue arrows, Fig. 2A, S1G), whereas the preferred direction of the grating receptive
243 field is horizontally to the right (red arrows, Fig. 2A, S1H). For comparison across neurons
244 we colour coded the preferred direction into four cardinal directions, and plotted them as a

245 function of receptive field centre location. This analysis shows that the preferred direction of
246 the target receptive fields was weakly correlated with location (Fig. 3A), with a slight
247 preference for motion away from the visual midline (Fig. 3C). In contrast, the directionality
248 of the grating receptive fields was strongly correlated with centre location (Fig. 3B), with a
249 strong dominance for motion away from the visual midline (Fig. 3D).

250 We next quantified the difference between the preferred directions of the target and the
251 grating receptive fields. In the example neuron, this is 141° (bottom right pictogram, Fig. 2A,
252 see also Fig. S1G, H). Across neurons there was a slight preference for similar directionality
253 in the two receptive fields, albeit with neurons encompassing the entire span of possible
254 directionality differences (Fig. 3E, see also Fig. S2). There was no distribution difference
255 based on whether the two receptive field centres were on the same side (grey, Fig. 3E) or
256 opposite sides (black, Fig. 3E) of the visual midline.

257 *Leading-edge sensitivity matches grating receptive field*

258 These descending neurons thus have two receptive fields, one that responds to small target
259 motion (blue, Fig. 2, S1, S2) and one that responds to local sinusoidal gratings (red, Fig. 2,
260 S1, S2). Which one of these receptive fields is most likely to contribute to their looming
261 sensitivity (right, Fig. 1)? Looming sensitive neurons in *Drosophila,* including the giant fiber,
262 also respond strongly to high-contrast bars and sweeping high-contrast edges (35). We thus
263 used full screen OFF edges to map the looming receptive field (Fig. S3). An example neuron
264 shows strong responses to an OFF edge sweeping either left (Fig. S3A), down (Fig. S3C), or
265 up (Fig. S3D) across the visual field, but not right (Fig. S3B). The resulting leading-edge
266 receptive field (cyan, Fig. S3E, F) overlaps substantially with the grating receptive field (red,
267 Fig. S3F), but not the target receptive field (blue, Fig. S3F).

268 Across neurons we compared the location of the leading-edge, the target, and the grating
269 receptive field centres (circles, Fig. 4A, S3F). A qualitative analysis shows that the leading-
270 edge receptive field centres tend to cluster below the visual equator, just like the grating
271 receptive field centres (cyan and red, Fig. 4A). For quantification, we calculated a proximity
272 index (Fig. 4B). When the leading-edge receptive field centre is closer to the grating
273 receptive field centre the proximity index is positive, with values close to 100% indicating
274 that they are much closer than to the target receptive field centre. In the example neuron, the
275 proximity index is 83% (Fig. 4B, S3). Across neurons, we found that the leading-edge
276 receptive field centre was frequently closer to the grating receptive field centre (red, Fig. 4C).
277 In those neurons where it was closer to the target receptive field centre, the proximity index
278 was relatively low (blue, Fig. 4C). In summary, it is likely that these neurons get their
279 looming sensitivity predominantly within the ventral visual field, overlapping with the
280 location of the grating receptive field.

281 *Different size response function in the two receptive fields*

282 Our previous work showed that looming sensitive neurons have a peculiar size response
283 function, with one peak to bars of a few degrees height, similar to the size tuning of target
284 selective neurons, and a second peak to full-screen bars (9). To investigate if this size
285 sensitivity differs between the two receptive fields we scanned bars of fixed width across the
286 visual monitor, while varying the height. We used two different trajectories, one centred on
287 the target receptive field (blue, Fig. 5A, S4), and one on the grating receptive field (red, Fig.
288 5A, S4). We found that the neurons responded strongly to small bars moving through the
289 target receptive field (blue, Fig. 5A, Fig. S4A-E), but not through the grating receptive field
290 (red, Fig. 5A, Fig. S4A-E). For the middle sized bars, the neurons responded weakly whether
291 they traversed the target or the grating receptive field (Fig. 5A, S4F-I).

292 When the bars were extended to cover a large part of the screen, they traversed both receptive
293 fields (Fig. S4J, K), making it hard to determine which receptive field the strong response
294 came from (Fig. 5A). To bypass this, we scanned the bars vertically instead of horizontally,
295 so that they traversed the grating receptive field and the target receptive field at different
296 points in time (pictogram, Fig. 5B, S5). We found that the neurons responded strongly when
297 small bars moved through the target analysis window (blue, Fig. 5B, S5A-E), and strongly to
298 large bars when they moved through the grating analysis window (red, Fig. 5B, S5G-L). This
299 shows that the target receptive field is tuned to small targets, whereas the grating receptive
300 field responds better to full-screen bars.

301 *Separate inputs to the two receptive fields*

302 The data above show that looming neurons have two receptive fields (Fig. 2-4), with size
303 tuning, suggesting that they receive separate input (Fig. 5). What happens when they are
304 stimulated simultaneously? To investigate this, we first determined the response when the
305 two receptive fields were stimulated separately, by scanning a small target through the target
306 receptive field (blue, Fig. 6A), and a series of bars through the grating receptive field (red,
307 Fig. 6A, consistent with the data in Fig. 5). We compared this to the response to simultaneous
308 stimulation (black, Fig. 6B). Interestingly, the response to simultaneous presentation (black,
309 Fig. 6B) was smaller than the linear sum of the two independent presentations (purple, Fig.
310 6B). Importantly, this cannot be due to response saturation, as the linear sum to the smallest
311 bars (purple, Fig. 6B) is on par with the measured response to the largest bars (black, Fig.
312 6B).

313 An alternative hypothesis is that the neuron selectively attends to one of the objects (36),
314 either the small target in the target receptive field, or the bar in the grating receptive field. We
315 investigated this by comparing the biggest response for each neuron (green, Fig. 6C), whether

316 that would be to the target or the bar, with the response to the simultaneous presentation
317 (black, Fig. 6C). We found that while there was a significant dependence on bar size, there
318 was no significant difference between the two conditions (compare green and black, Fig. 6C,
319 2-way ANOVA), suggesting that the neuron could be selectively attending to one of the
320 objects and ignoring the other.

321 *Target receptive field is based on 1-point correlator input, whereas the grating receptive*
322 *field uses 2-point correlator input*

323 The data above show two independent receptive fields. What is the likely pre-synaptic input
324 to each? Both optic lobe and descending target tuned neurons (37, 38) generate their target
325 selectivity using 1-point correlators, which are based on the comparison of an OFF contrast
326 change immediately followed by an ON contrast change at a single point in space (39). These
327 correlators are fundamentally different from 2-point correlators, such as Hassenstein-
328 Reichard elementary motion detectors (40), in their response to high-contrast edges. For
329 example, a 1-point correlator will respond only weakly to either OFF or ON contrast edges,
330 compared with complete objects, whereas 2-point correlators respond equally well to single
331 edges and complete objects (inset, Fig. 7, data replotted from Ref. 37).

332 To investigate the potential input to the two receptive fields we first scanned an OFF edge
333 through the grating receptive field, then an ON edge, followed by a complete bar (red, Fig.
334 7). We found that the responses to single edges were similar to the response to a complete bar
335 (ns, red, Fig. 7). The response was consistent with an underlying 2-point correlator input
336 (compare red data with inset, Fig. 7). In contrast, when we scanned edges or targets through
337 the target receptive field, the response to a complete target was much stronger than to either
338 OFF or ON edges on their own ($P < 0.0001$, blue, Fig. 7). Indeed, the response was consistent
339 with an underlying 1-point correlator input (compare blue data with inset, Fig. 7). In response

340 to full-screen edges and bars, which cover both receptive fields, we found the strongest
341 response to the OFF edge (P = 0.0049 for OFF vs bar, ns for ON vs bar, black, Fig. 7).

342 Discussion

343 We have shown here a group of descending neurons in the hoverfly *Eristalis tenax* that are
344 sensitive to both targets and to looming stimuli (Fig. 1). We show that this dual sensitivity
345 originates from two discrete receptive fields, with different locations (Fig. 2, S1E, F, S2) and
346 preferred directions (Fig. 3, S1G, H, S2). We show that the looming sensitivity is likely
347 associated with the ventral receptive field (Fig. 4, S3). The size tuning (Fig. 5, S4, S5) and
348 sensitivity to OFF and ON contrast edges (Fig. 7) supports independent input to the two
349 receptive fields, using two fundamentally different pre-synaptic pathways. Interestingly, the
350 input from the two pathways is not linearly summed (Fig. 6B) but could be subject to
351 selective attention (Fig. 6C), as previously shown in dragonfly target neurons (36).

352 *Dual receptive fields*

353 The neurons that we describe here were classified as looming sensitive based on a strong
354 response to a looming stimulus (right, Fig. 1) compared with an appearance control (9).
355 However, as they also respond strongly to small moving targets (left, Fig. 1, Fig. 5), they
356 could have been classified as target selective descending neurons (TSDN). Indeed, the
357 dragonfly TSDN DIT3 responds strongly to both small targets and to looming stimuli (21). In
358 the locust, LGMD/DCMD neurons respond to both targets and to looming stimuli (16), and
359 some central complex looming sensitive neurons also respond to small moving targets (20).
360 Similarly, in *Drosophila,* some optic lobe and descending looming sensitive neurons also
361 respond to smaller objects (e.g. 17, 35, 41, 42).

362 However, as opposed to these examples (e.g. 16, 20, 21, 35), we show that the dual
363 sensitivity to small targets and to larger objects comes from two discrete receptive fields (Fig.
364 2 – 4, S1 – S3). It is currently unknown if the dual sensitivity described in other insects (e.g.
365 16, 20, 21, 35) also comes from different receptive fields. Interestingly, *Drosophila* Foma-1
366 responds to small flickering targets (10° diameter) in addition to looming stimuli (17). While
367 the visual field location of the looming sensitivity was not specified, target sensitivity was
368 specific to the dorsal visual field (17), similar to our data (blue, Fig. 2B, C).

369 Our recordings were done extracellularly (Fig. 1), meaning that neurons with no spontaneous
370 activity are difficult to discover without presenting a suitable stimulus. We used a small
371 moving target to initially identify visual neurons (left, Fig. 1), thus biasing our results
372 towards those looming sensitive descending neurons that also responded to small targets.
373 However, it is likely that there are looming neurons that do not respond to small objects, such
374 as found in e.g. *Drosophila* (e.g. 42, 43) and crabs (see e.g. 44). Additionally, our visual
375 monitor was placed in front of the animal, thus biasing our results to neurons with frontal
376 sensitivity. It is likely that there are additional looming sensitive descending neurons with
377 dorsal receptive fields, which could be useful for e.g. detecting predators approaching from
378 above, or lateral receptive fields, which could be useful for avoiding imminent collision. For
379 example, in the crab there are 16 retinotopically arranged looming sensitive MLGs that
380 underlie directional escape behaviours (45). While each receptive field is small, together the
381 16 neurons cover 360° of the visual field (45), and are thus able to encode directional escape
382 responses.

383 *Neuronal mechanisms*

384 We showed that the looming sensitive descending neurons likely receive distinct input to the
385 two receptive fields (Fig. 5-7). Indeed, the dorsal target receptive field is likely to use pre-

synaptic 1-point correlators (blue, Fig. 7), just like the TSDNs do (38). Furthermore, the size tuning of the dorsal target receptive field (blue, Fig. 5, S4-5) is similar to the size tuning of TSDNs (38, 46), and of the presumably pre-synaptic STMDs (47). This suggests that the dorsal target receptive field could share input with the TSDNs.

In contrast, the ventral grating receptive field responded better to larger bars than to small targets (red, Fig. 5, S4-5), similar to optic flow sensitive descending neurons (38). In addition, the ventral grating receptive field is likely to use pre-synaptic 2-point correlators of the EMD-type (red, Fig. 7), similar to optic flow sensitive neurons (48). Interestingly, the looming sensitive LPLC2 neurons, which are pre-synaptic to the *Drosophila* giant fiber (43), get their input from T4/T5 (42), which is consistent with a 2-point, EMD-type, correlator input (see e.g. 49). As our leading-edge data suggests that looming sensitivity is associated with the grating receptive field (Fig. 4, S3), this indicates that looming sensitivity could be generated by 2-point correlation. Indeed, in the housefly, escapes can be triggered by widefield gratings, even if not as efficiently as by looming stimuli (50).

We found that the directionality of the grating receptive field was strongly correlated with the azimuthal location of the receptive field centre (Fig. 3B, D). However, the directionality of the target receptive field was much less dependent on its visual field location (Fig. 3A, C). In addition, we found no correlation between the direction tuning of the two receptive fields (Fig. 3E). We also found that when both receptive fields were stimulated, the response could not be explained by a linear summation of the responses to the two stimuli on their own (Fig. 6B), again highlighting that the two receptive fields likely receive independent input. Similarly, the locust LGMD (51) displays non-linear interactions when stimuli are placed in different parts of the visual field, suggesting that the details of its receptive fields may be worth investigating in the future.

Behavioural role

Previous work has shown that the same stimulus displayed in different parts of the visual field can elicit different behavioural output. For example, when crabs living in mudflats see a small dummy moved at ground level they initiate prey pursuit behaviour, but when the same dummy is moved above the crab, they try to escape it (52). In flying *Drosophila*, a looming stimulus in the lateral visual field leads to an escape response, whereas a looming stimulus in the frontal visual field leads to landing behaviour (53). While we did not stimulate the lateral visual field in our set-ups, the strong responses to frontal looming stimuli (right, Fig. 1), likely associated with the ventral receptive field (Fig. 4), suggests that this could be used during landing behaviours on e.g. flowers. Indeed, bees adjust their body angle when landing so the landing surface ends up in the ventral visual field (54).

However, the neurons that we described here could be even more useful in pursuit behaviours. Indeed, when a hoverfly is pursuing a target, during most of the pursuit it will be projected as a small object on the pursuer's eye (55). If the hoverfly were below the target during this part of the pursuit, having a dorsal target receptive field would be appropriate (blue, Fig. 2A-C). This part of the pursuit could thus be supported by either the neurons described here, or by TSDNs without looming sensitivity (9, 38, 46).

During later stages of the pursuit, when the hoverfly gets closer to the target, this will be seen as a looming object (7). Indeed, it has been suggested that this part of the pursuit cannot be subserved by classic target tuned neurons, but instead requires neurons that respond to larger objects and looming stimuli (see e.g. Discussion in Ref. 11), like in zebrafish larvae (12). Furthermore, during the final stages before capture, the pursuer would need to orient itself to grab the target with its legs. During this stage the target would be seen as a large object in the ventral visual field, which would make the more ventral receptive field useful (red, Fig. 2A-

C). In *Drosophila*, looming sensitive Foma-1 is not only involved in escape responses if the fly is stationary (17), but also in courtship, where its silencing results in male flies not being able to follow females (27). Future work investigating where the neurons described here project to, and which behaviours they are thus likely to control, will help elucidate this.

Acknowledgements

We thank past and current lab members for constructive feedback, and the Botanic Gardens of Adelaide for their ongoing support. This research was funded by the US Air Force Office of Scientific Research (AFOSR, FA9550-19-1-0294), the Australian Research Council (ARC, DP180100144, DP210100740 and FT180100289).

References

1. R. M. Olberg, R. C. Seaman, M. I. Coats, A. F. Henry, Eye movements and target fixation during dragonfly prey-interception flights. *J Comp Physiol A* **193**, 685-693 (2007).
2. S. T. Fabian, M. E. Sumner, T. J. Wardill, S. Rossoni, P. T. Gonzalez-Bellido, Interception by two predatory fly species is explained by a proportional navigation feedback controller. *Journal of The Royal Society Interface* **15** (2018).
3. V. Nityananda *et al.*, Insect stereopsis demonstrated using a 3D insect cinema. *Sci Rep* **6**, 18718 (2016).
4. S. M. Fitzpatrick, W. G. Wellington, Contrasts in the territorial behavior of three species of hover flies (Diptera: Syrphidae). *Can Entomol* **115**, 559-566 (1983).
5. J. Zeil, The territorial flight of male houseflies (*Fannia canicularis* L.). *Behav Ecol Sociobiol* **19**, 312-219 (1986).
6. N. Boeddeker, R. Kern, M. Egelhaaf, Chasing a dummy target: smooth pursuit and velocity control in male blowflies. *Proc Biol Sci* **270**, 393-399 (2003).
7. M. Thyselius *et al.*, Male hoverflies (*Eristalis tenax*) do not use heuristic rules based on retinal size and speed during indoor pursuits of artificial targets. *bioRxiv* 10.1101/2022.07.27.501787, 2022.2007.2027.501787 (2022).
8. L. Varennes, H. G. Krapp, S. Viollet, Two pursuit strategies for a single sensorimotor control task in blowfly. *Sci Rep* **10**, 20762 (2020).
9. S. Nicholas, R. Leibbrandt, K. Nordström, Visual motion sensitivity in descending neurons in the hoverfly. *J Comp Physiol A* **206**, 149-163 (2020).
10. K. Nordström, P. D. Barnett, D. C. O'Carroll, Insect detection of small targets moving in visual clutter. *PLoS Biol* **4**, 378-386 (2006).

11. Z. M. Bagheri, S. D. Wiederman, B. S. Cazzolato, S. Grainger, D. C. O'Carroll, Properties of neuronal facilitation that improve target tracking in natural pursuit simulations. *J Roy Soc Interface* **12**, 20150083 (2015).

12. P. M. Henriques, N. Rahman, S. E. Jackson, I. H. Bianco, Nucleus Isthmi Is Required to Sustain Target Pursuit during Visually Guided Prey-Catching. *Current Biology* **29**, 1771-1786.e1775 (2019).

13. Y. J. Liu, Q. Wang, B. Li, Neuronal responses to looming objects in the superior colliculus of the cat. *Brain Behav Evol* **77**, 193-205 (2011).

14. H. Nakagawa, K. Hongjian, Collision-sensitive neurons in the optic tectum of the bullfrog, Rana catesbeiana. *J Neurophysiol* **104**, 2487-2499 (2010).

15. I. Temizer, J. C. Donovan, H. Baier, J. L. Semmelhack, A visual pathway for looming-evoked escape in larval zebrafish. *Curr Biol* **25**, 1823-1834 (2015).

16. R. D. Santer, F. C. Rind, P. J. Simmons, Predator versus prey: locust looming-detector neuron and behavioural responses to stimuli representing attacking bird predators. *PLoS One* **7**, e50146 (2012).

17. S. E. de Vries, T. R. Clandinin, Loom-sensitive neurons link computation to action in the *Drosophila* visual system. *Curr Biol* **22**, 353-362 (2012).

18. H. Fotowat, A. Fayyazuddin, H. J. Bellen, F. Gabbiani, A novel neuronal pathway for visually guided escape in *Drosophila melanogaster*. *J Neurophysiol* **102**, 875-885 (2009).

19. F. C. Rind, P. J. Simmons, Orthopteran DCMD neuron: A re-evaluation of responses to moving objects. I. Selective responses to approaching objects. *J Neurophysiol* **68**, 1654-1666 (1992).

20. R. Rosner, U. Homberg, Widespread sensitivity to looming stimuli and small moving objects in the central complex of an insect brain. *J Neurosci* **33**, 8122-8133 (2013).

21. P. T. Gonzalez-Bellido, H. Peng, J. Yang, A. P. Georgopoulos, R. M. Olberg, Eight pairs of descending neurons in the dragonfly give wing motor centres accurate population vector of prey direction. *Proc Natl Acad Sci USA* **110**, 676-701 (2013).

22. M. A. Frye, R. M. Olberg, Visual receptive field properties of feature detecting neurons in the dragonfly. *J Comp Physiol A* **177**, 569-576 (1995).

23. C. R. von Reyn *et al.*, Feature Integration Drives Probabilistic Behavior in the Drosophila Escape Response. *Neuron* **94**, 1190-1204.e1196 (2017).

24. D. S. Mearns, J. C. Donovan, A. M. Fernandes, J. L. Semmelhack, H. Baier, Deconstructing hunting behavior reveals a tightly coupled stimulus-response loop. *Curr Biol* **30**, 54-69.e59 (2020).

25. B. W. Patterson, A. O. Abraham, M. A. MacIver, D. L. McLean, Visually guided gradation of prey capture movements in larval zebrafish. *J Exp Biol* **216**, 3071-3083 (2013).

26. D. Förster *et al.*, Retinotectal circuitry of larval zebrafish is adapted to detection and pursuit of prey. *eLife* **9**, e58596 (2020).

27. P. Coen, M. Xie, J. Clemens, M. Murthy, Sensorimotor transformations underlying variability in song intensity during *Drosophila* courtship. *Neuron* **89**, 629-644 (2016).

28. R. D. Santer, Y. Yamawaki, F. C. Rind, P. J. Simmons, Preparing for escape: an examination of the role of the DCMD neuron in locust escape jumps. *J Comp Physiol A Neuroethol Sens Neural Behav Physiol* **194**, 69-77 (2008).

29. S. Nicholas, M. Thyselius, M. Holden, K. Nordström, Rearing and long-term maintenance of *Eristalis tenax* hoverflies for research studies. *JoVE* doi:10.3791/57711, e57711 (2018).

30. D. H. Brainard, The Psychophysics toolbox. *Spatial Vision* **10**, 433-436 (1997).

31. D. G. Pelli, The VideoToolbox software for visual psychophysics: Transforming numbers into movies. *Spatial Vision* **10**, 437-442 (1997).

32. H. Fotowat, F. Gabbiani, Relationship between the phases of sensory and motor activity during a looming-evoked multistage escape behavior. *J Neurosci* **27**, 10047-10059 (2007).

33. K. Nordström, I. M. Moyer de Miguel, D. C. O'Carroll, Rapid contrast gain reduction following motion adaptation. *J Exp Biol* **214**, 4000-4009 (2011).

34. K. Nordström, D. C. O'Carroll, The motion after-effect: Local and global contributions to contrast sensitivity. *Proc R Soc Lond B* **276**, 1545-1554 (2009).

35. J. M. Ache, S. Namiki, A. Lee, K. Branson, G. M. Card, State-dependent decoupling of sensory and motor circuits underlies behavioral flexibility in *Drosophila*. *Nat Neurosci* **22**, 1132-1139 (2019).

36. S. D. Wiederman, D. C. O'Carroll, Selective attention in an insect visual neuron. *Curr Biol* **23**, 156-161 (2013).

37. S. D. Wiederman, P. A. Shoemaker, D. C. O'Carroll, Correlation between OFF and ON Channels Underlies Dark Target Selectivity in an Insect Visual System. *J Neurosci* **33**, 13225-13232 (2013).

38. S. Nicholas, K. Nordström, Facilitation of neural responses to targets moving against optic flow. *Proc Natl Acad Sci U S A* **118** (2021).

39. S. D. Wiederman, P. A. Shoemaker, D. C. O'Carroll, A model for the detection of moving targets in visual clutter inspired by insect physiology. *PLoS ONE* **3**, e2784 (2008).

40. B. Hassenstein, W. Reichardt, Systemtheoretische Analyse der Zeit, Reihenfolgen und Vorzeichenauswertung Bei der Bewegungsperzeption des Rüsselkafers *Chlorophanus*. *Z Naturforsch* **11**, 513-524 (1956).

41. S. Namiki, M. H. Dickinson, A. M. Wong, W. Korff, G. M. Card, The functional organization of descending sensory-motor pathways in *Drosophila*. *eLife* **7**, e34272 (2018).

42. N. C. Klapoetke *et al.*, Ultra-selective looming detection from radial motion opponency. *Nature* **551**, 237-241 (2017).

43. J. M. Ache *et al.*, Neural basis for looming size and velocity encoding in the *Drosophila* Giant Fiber escape pathway. *Curr Biol* **29**, 1073-1081.e1074 (2019).

44. A. Cámera, M. A. Belluscio, D. Tomsic, Multielectrode Recordings From Identified Neurons Involved in Visually Elicited Escape Behavior. *Front Behav Neurosci* **14**, 592309 (2020).

45. V. Medan, M. Beron De Astrada, F. Scarano, D. Tomsic, A network of visual motion-sensitive neurons for computing object position in an arthropod. *J Neurosci* **35**, 6654-6666 (2015).

46. S. Nicholas, J. Supple, R. Leibbrandt, P. T. Gonzalez-Bellido, K. Nordström, Integration of small- and wide-field visual features in Target-Selective Descending Neurons of both predatory and non-predatory dipterans. *J Neurosci* **38**, 10725-10733 (2018).

47. K. Nordström, Neural specializations for small target detection in insects. *Curr Opin Neurobiol* **22**, 272-278 (2012).

48. R. A. Harris, D. C. O'Carroll, S. B. Laughlin, Adaptation and the temporal delay filter of fly motion detectors. *Vision Res* **39**, 2603-2613. (1999).

49. E. Salazar-Gatzimas *et al.*, Direct Measurement of Correlation Responses in Drosophila Elementary Motion Detectors Reveals Fast Timescale Tuning. *Neuron* **92**, 227-239 (2016).

566 50. M. H. Holmqvist, M. V. Srinivasan, A visually evoked escape response of the
567 housefly. *J Comp Physiol A* **169**, 451-459 (1991).
568 51. H. G. Krapp, F. Gabbiani, Spatial Distribution of Inputs and Local Receptive Field
569 Properties of a Wide-Field, Looming Sensitive Neuron. *Journal of Neurophysiology*
570 **93**, 2240-2253 (2005).
571 52. D. Tomsic, J. Sztarker, M. Berón de Astrada, D. Oliva, E. Lanza, The predator and
572 prey behaviors of crabs: from ecology to neural adaptations. *Journal of Experimental*
573 *Biology* **220**, 2318-2327 (2017).
574 53. L. F. Tammero, M. H. Dickinson, Collision-avoidance and landing responses are
575 mediated by separate pathways in the fruit fly, *Drosophila melanogaster*. *J Exp Biol*
576 **205**, 2785-2798 (2002).
577 54. C. Evangelista, P. Kraft, M. Dacke, J. Reinhard, M. V. Srinivasan, The moment
578 before touchdown: landing manoeuvres of the honeybee Apis mellifera. *Journal of*
579 *Experimental Biology* **213**, 262-270 (2010).
580 55. P. T. Gonzalez-Bellido, S. T. Fabian, K. Nordström, Target detection in insects:
581 optical, neural and behavioral optimizations. *Curr Opin Neurobiol* **41**, 122-128
582 (2016).
583

584

585 ## Figure Legends

586 ***Figure 1. Looming sensitive descending neurons respond robustly to looming stimuli and***
587 ***to small targets.*** **A)** Pictograms of the 3° × 3° square target moving horizontally (*Left*) and
588 the looming stimulus with an l/|v| of 10 ms and a final size of 117° (*Right*), as projected on
589 the frontal visual monitor. **B)** Raw data trace from an extracellular recording of a looming
590 sensitive descending neuron in response to a small target (*Left*) or a looming stimulus (*Right*).
591 **C)** The position of the target on the visual monitor (*Left*) and the diameter of the looming
592 stimulus (*Right*), time aligned with the data in panel B. **D)** Spike histograms of the responses
593 in panel B using 20 ms bins.

594 ***Figure 2. Two different receptive fields.*** **A)** The location of the two receptive fields of an
595 example neuron as projected onto the visual monitor. The outlines show the 50% response
596 and the small circle the centre of the target receptive field (blue) and the grating receptive
597 field (red). Euclidean distance between the receptive field centres (black line and value) and
598 the distance of each receptive field centre to the equator and the visual midline (coloured
599 lines and values) are indicated. Bottom right pictogram indicates the preferred direction of
600 the target (blue arrow) and the grating receptive field (red arrow), and the difference between
601 the two (black arc and value). **B)** Location of target (blue) and grating receptive field centres
602 (red) across 102 neurons. **C)** Vertical distance between target (blue) and grating receptive
603 field centres (red) and the visual equator (10° bins). **D)** Horizontal distance from the visual
604 midline (10° bins). **E)** Euclidean distance between each neuron's two receptive field centres
605 (10° bins). Grey data come from neurons where the target receptive field was dorsal to the
606 grating receptive field centre (N = 90) and black data from neurons where the grating
607 receptive field was dorsal to the target receptive field centre (N = 12).

608 ***Figure 3. The preferred direction depends on the receptive field centre location.*** **A)** The
609 target receptive field centres, colour coded according to their preferred direction (pictogram
610 bottom right). **B)** The grating receptive field centres, colour coded according to their
611 preferred direction. **C)** Preferred direction of target receptive fields with centres in either the
612 left or the right visual field (30° bins). **D)** Preferred direction of grating receptive fields
613 centres in either the left or the right visual field (30° bins). **E)** Preferred direction difference
614 between the target and grating receptive field of each neuron (10° bins). Grey data show
615 neurons where the two receptive field centres were on the same side of the visual midline
616 (N = 93), whereas black data show neurons with receptive fields on opposite sides of the
617 visual midline (N = 9).

618 ***Figure 4. The leading-edge receptive field is closer to the grating receptive field.*** **A)** The
619 location of the target (blue), grating (red) and leading-edge (cyan) receptive field centres in
620 15 neurons. **B)** The receptive field centres for one example neuron (*Left*), with distances
621 (black lines) between the leading-edge and the target receptive field centre (*d1*), or the
622 grating receptive field centre (*d2*), used to calculate the proximity index (*Right*). **C)** Leading
623 edge proximity index across neurons (N = 15). The leading-edge receptive field was closer to
624 the grating receptive field centre (red) in more neurons (N = 12) than to the target receptive
625 field (blue, N = 3). The distribution was significantly different from 0 ($P < 0.01$, one sample t
626 and Wilcoxon signed rank test).

627 ***Figure 5. The two receptive fields have different size response functions.*** **A)** The pictograms
628 indicate the bar trajectory as it moved horizontally across the screen, subtending either the
629 target receptive field (*Left*, blue dashed line and arrow) or the grating receptive field (*Right*,
630 red dashed line and arrow, example bar height is 84°). Typical target and grating receptive
631 fields for an example neuron are shown. The grey shading shows the analysis window used to

632 calculate the mean response rate, which is the same for both trajectories. The graph shows
633 that responses to small bars are significantly stronger when passing through the target
634 receptive field (blue) compared to the grating receptive field (red, mean ± SEM, N = 8). **B)**
635 The pictogram indicates the analysis windows used to calculate the response to a bar of
636 varying width as it moved vertically along the screen (trajectory in black) subtending the
637 target receptive field (blue) or the grating receptive field (red). The graph shows that
638 responses to narrow bars are significantly stronger within the target analysis window (AW,
639 blue), while responses to wider bars are significantly stronger within the grating analysis
640 window (red, mean ± SEM, N = 10). Statistical test was a two-way ANOVA followed by
641 Sidak's multiple comparisons, with ****P < 0.0001, ***P < 0.001, **P < 0.01 and *P <
642 0.05.

643 ***Figure 6. Response to simultaneous stimulation of the two receptive fields.*** **A)** Responses to
644 a small target traversing the target receptive field (blue), or bars of varying heights traversing
645 the grating receptive field (red). The pictograms at the top show the screen position of each
646 trajectory in relation to the receptive fields for an example neuron. Grey shading indicated the
647 analysis window used to calculate the mean response rate. **B)** Pictogram showing the screen
648 position of simultaneously presented target and bar traversing the target and grating receptive
649 fields. The graph shows that the responses to simultaneous presentation (black) are
650 significantly lower than the sum of the responses to the same stimuli presented on their own
651 (purple). **C)** The responses to simultaneous stimuli (black) are not significantly different from
652 the strongest response evoked by either the target or the bar on its own (green). For all panels
653 the data show mean ± SEM, for the same N = 5. Statistical analysis was done using two-way
654 ANOVA, with ****P < 0.0001, **P < 0.01 and ns indicating P > 0.05.

Figure 7. These looming neurons get input from both 1- and 2-point correlators. The response to a leading OFF edge, a trailing ON edge, or a complete bar, all with a height of 84°, traversing the grating receptive field (red, N = 9), a height of 3° traversing the target receptive field (blue, N = 10), or the full height of the screen (black, N = 7). The stimuli moved horizontally at a velocity of 900 pixels/s. In all cases the response from each neuron was normalized to the sum of the response to all three stimuli from the same trajectory (i.e. OFF edge only, ON edge only, or complete bar). The inset shows the predicted response of a motion detector that compares luminance changes over one point (also referred to as an elementary STMD) or two points in space (often referred to as an EMD). The inset pictograms are replotted from (37).

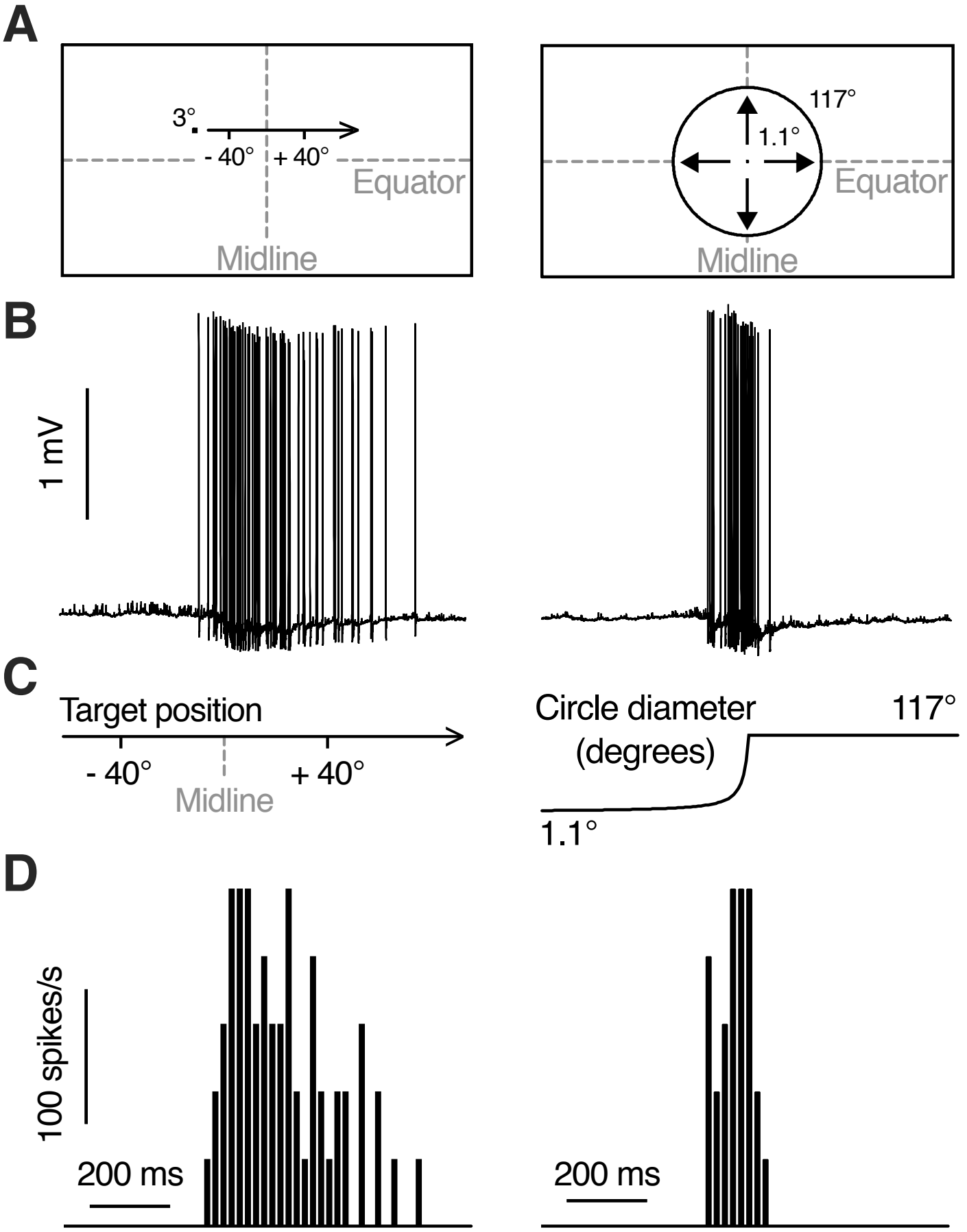
A
3°
- 40°
+ 40°
Equator
Midline
117°
1.1°
Equator
Midline
B
1 mV
C
Target position
- 40°
+ 40°
Midline
Circle diameter
(degrees)
117°
1.1°
D
100 spikes/s
200 ms
200 ms

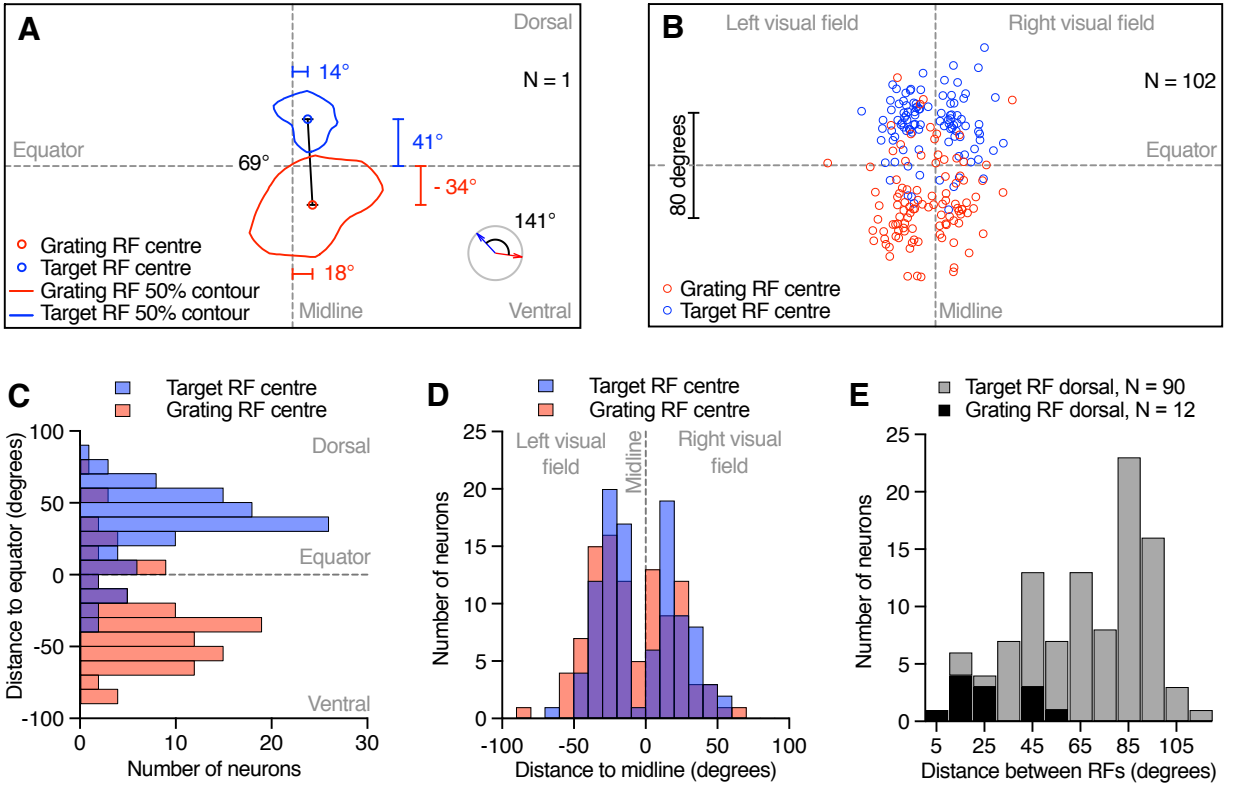
A
Dorsal
N = 1
14°
41°
Equator
69°
- 34°
141°
18°
Grating RF centre
Target RF centre
Grating RF 50% contour
Target RF 50% contour
Midline
Ventral
B
Left visual field
Right visual field
N = 102
80 degrees
Equator
Grating RF centre
Target RF centre
Midline
C
Target RF centre
Grating RF centre
Dorsal
Equator
Ventral
Distance to equator (degrees)
Number of neurons
D
Target RF centre
Grating RF centre
Left visual field
Midline
Right visual field
Number of neurons
Distance to midline (degrees)
E
Target RF dorsal, N = 90
Grating RF dorsal, N = 12
Number of neurons
Distance between RFs (degrees)

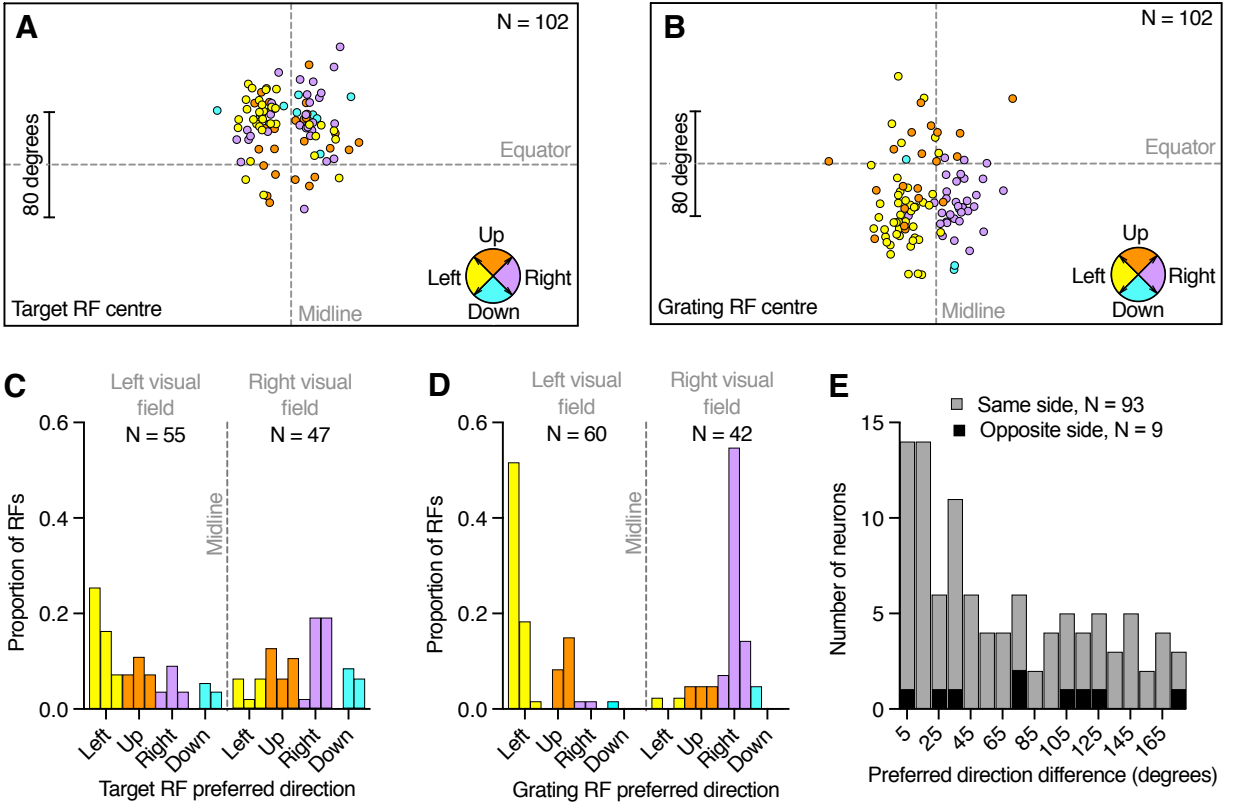
A
N = 102
80 degrees
Equator
Up
Left
Right
Down
Target RF centre
Midline
B
N = 102
80 degrees
Equator
Up
Left
Right
Down
Grating RF centre
Midline
C
Left visual field
N = 55
Right visual field
N = 47
Midline
Proportion of RFs
0.6
0.4
0.2
0.0
Left
Up
Right
Down
Left
Up
Right
Down
Target RF preferred direction
D
Left visual field
N = 60
Right visual field
N = 42
Midline
Proportion of RFs
0.6
0.4
0.2
0.0
Left
Up
Right
Down
Left
Up
Right
Down
Grating RF preferred direction
E
Same side, N = 93
Opposite side, N = 9
Number of neurons
15
10
5
0
5
25
45
65
85
105
125
145
165
Preferred direction difference (degrees)

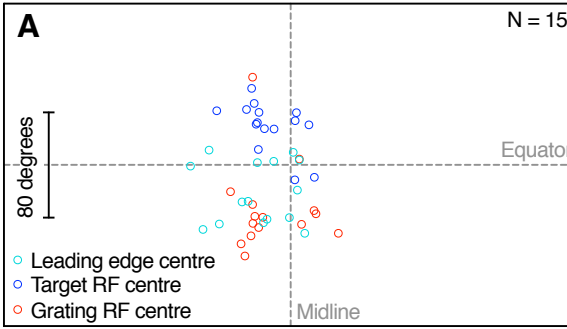
A
N = 15
80 degrees
Equator
Leading edge centre
Target RF centre
Grating RF centre
Midline

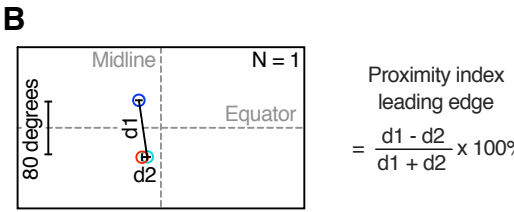
B
Midline
N = 1
80 degrees
Equator
d1
d2
Proximity index
leading edge
= (d1 - d2) / (d1 + d2) x 100%

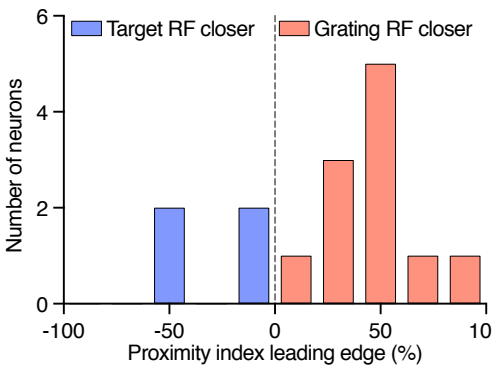
C
Target RF closer
Grating RF closer
Number of neurons
0
2
4
6
-100
-50
0
50
100
Proximity index leading edge (%)

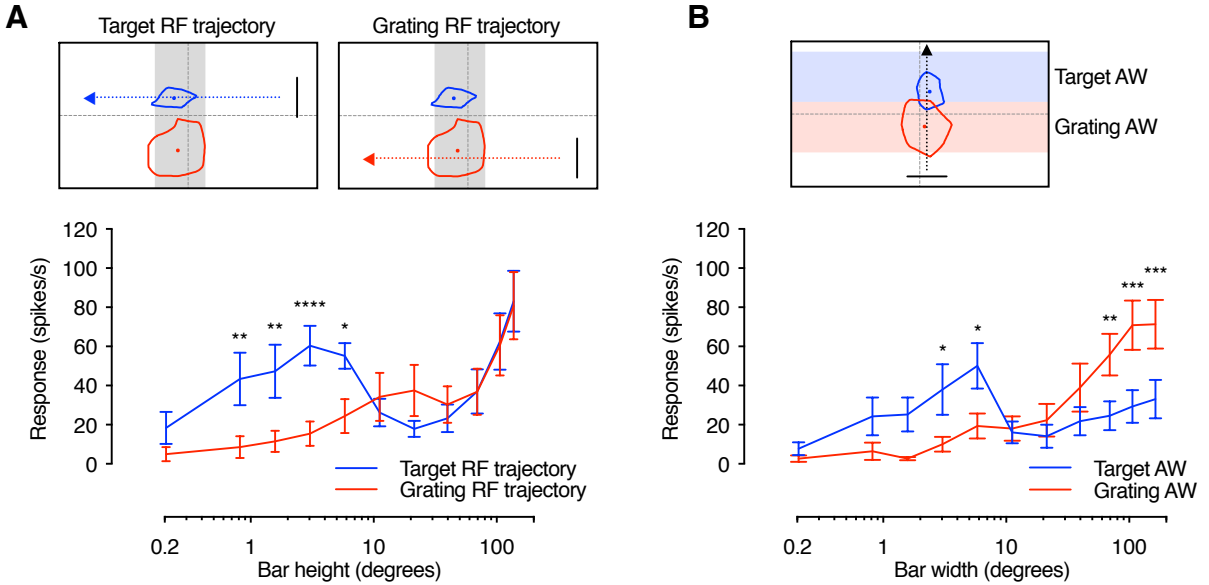
A
Target RF trajectory
Grating RF trajectory
Response (spikes/s)
120
100
80
60
40
20
0
**
**
****
*
Target RF trajectory
Grating RF trajectory
0.2
1
10
100
Bar height (degrees)
B
Target AW
Grating AW
Response (spikes/s)
120
100
80
60
40
20
0
*
*
**
***
***
Target AW
Grating AW
0.2
1
10
100
Bar width (degrees)

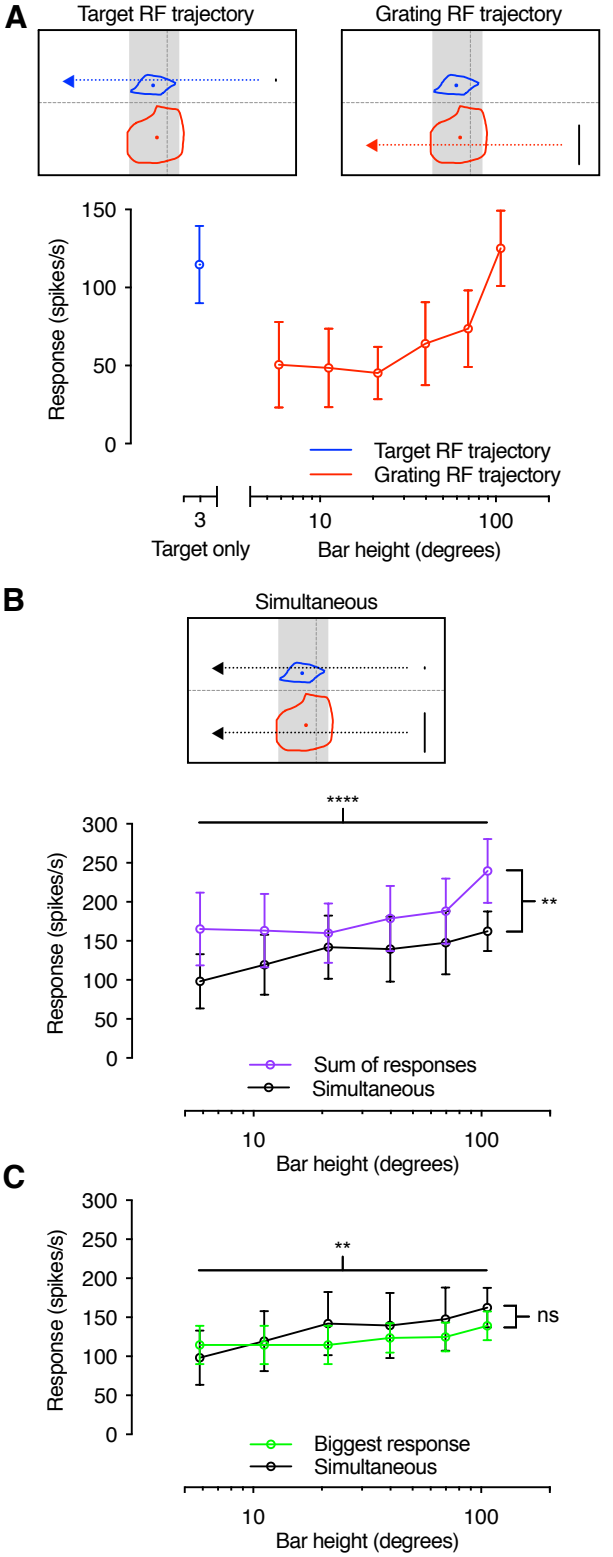
A
Target RF trajectory
Grating RF trajectory
Response (spikes/s)
150
100
50
0
Target RF trajectory
Grating RF trajectory
3
10
100
Target only
Bar height (degrees)
B
Simultaneous
Response (spikes/s)
300
250
200
150
100
50
0
****
**
Sum of responses
Simultaneous
10
100
Bar height (degrees)
C
Response (spikes/s)
300
250
200
150
100
50
0
**
ns
Biggest response
Simultaneous
10
100
Bar height (degrees)

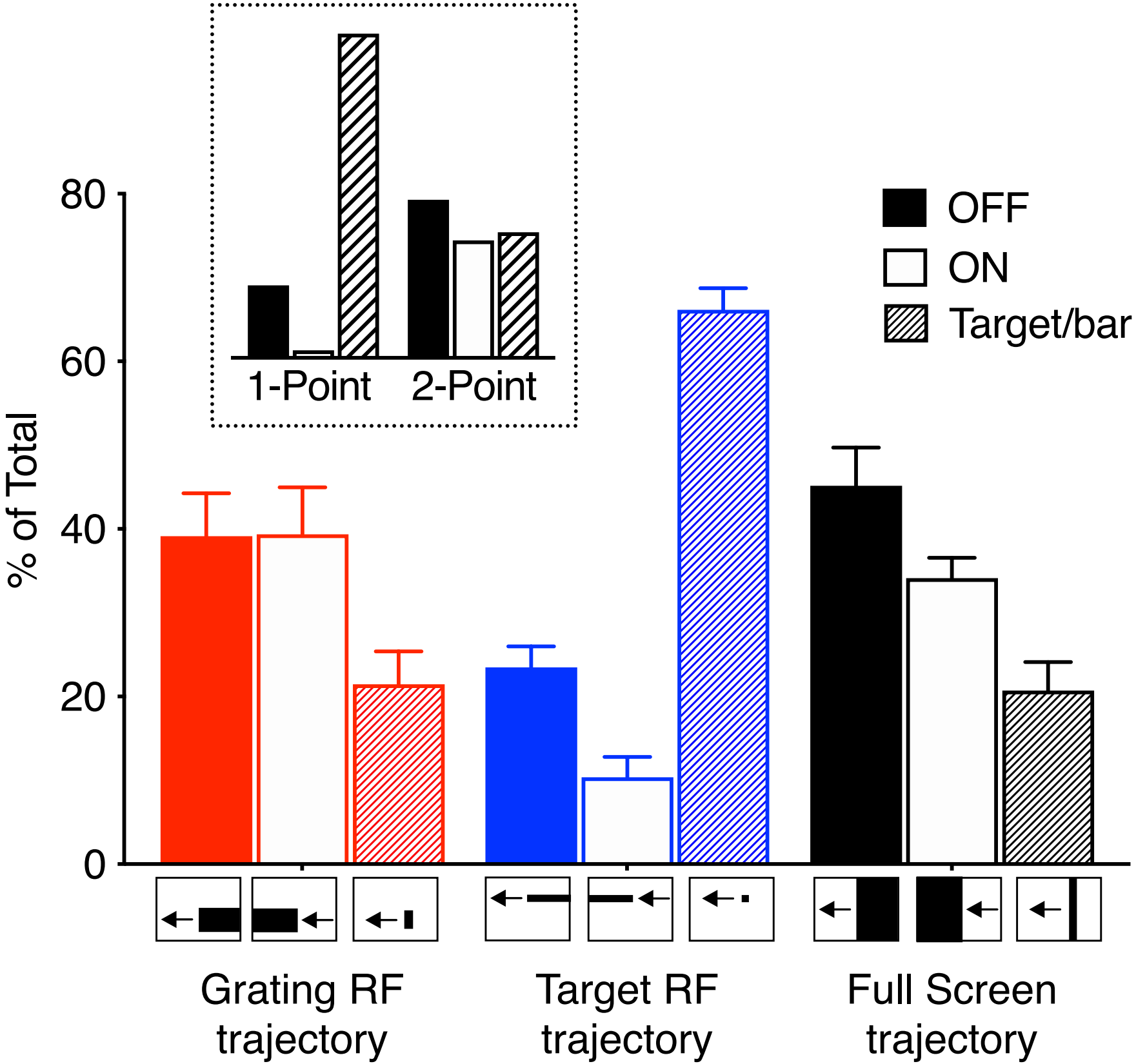
80
60
40
20
0
% of Total
1-Point
2-Point
OFF
ON
Target/bar
Grating RF trajectory
Target RF trajectory
Full Screen trajectory

Supplementary Information

Figure S1. Receptive field mapping method. **A)** The resulting 20 x 20 analysis windows after scanning the entire monitor along 20 evenly spaced horizontal and vertical target trajectories. The blue boxes highlight the positions of the analysis windows (P1 – 4) shown in panel C. **B)** The resulting 8 x 6 grid of overlapping patches of sinusoidal gratings. The red boxes highlight the grid locations (P1 – 4) shown in panel D. **C)** The responses (open symbols) to 4 directions of target motion within the analysis windows highlighted in panel A. We fit a cosine function (black) to the responses and used this to extract the local preferred direction (LPD, filled triangle), and local motion sensitivity (LMS, vertical bar). The dotted line shows the mean response. **D)** The responses (open symbols) to 8 different directions within the positions highlighted in panel B, the resulting cosine function (black), the local preferred direction (LPD, filled triangle), local motion sensitivity (LMS, vertical bar), and mean response (dotted line). **E)** The target receptive field's position, shown as contour lines (blue and grey). The centre position (blue circle) was defined as the centroid of the 50% contour line. **F)** The grating receptive field's position, shown as contour lines (red and grey), and its centre (red circle). **G)** The arrows show the local motion sensitivity (arrow length) and local preferred direction (arrow angle) of the target receptive field. Blue arrows indicate the preferred direction in positions where the local motion sensitivity was greater than 50% of the maximum for this neuron. Bottom right pictogram indicates the resulting average preferred direction. **H)** Local motion sensitivity and preferred direction of the grating receptive field. The bottom right pictogram indicates the average preferred direction (red). The data in this figure comes from the example neuron shown in Figure *2A*.

Figure S2. Looming sensitive descending neurons are a heterogeneous group of neurons. **A)** Target (blue) and grating (red) receptive field of an example neuron. The contour lines

show the 50% response, and the circles the centres of each receptive field. The arrows show the local preferred direction for positions where the response was >50% of the maximum local motion sensitivity. The bottom right pictogram indicates the average preferred direction for the target receptive field (blue) and grating receptive field (red), as well as the difference between the two (black arc and value). The Euclidean distance between the two receptive field centres (black line and value) is indicated on the left. **B)** Example of a looming sensitive neuron with small target and grating receptive fields, and a large distance between the centres. **C)** Example neuron with a large difference between their preferred directions. **D)** Example neuron where the grating receptive field is dorsal to the target receptive field. **E)** Example neuron where the grating receptive field is dorsal to the equator and overlapping with the target receptive field. **F)** Example neuron where the grating and target receptive fields are large and partially overlapping.

Figure S3. Leading edge receptive field method. **A)** Example response from a single neuron (mean +/- SEM) to a full screen OFF edge moving left across the entire width of the screen. Dashed purple line indicates 50% of the maximum response achieved to any direction of leading-edge motion in this neuron. Thresholds (cyan lines) are defined as the time when the neuronal response passes 50% of the maximal response. **B)** Neuronal response to an OFF edge moving right. As the response did not reach 50% maximum, thresholds were not achieved in this direction. **C)** Neuronal response to an OFF edge moving down. **D)** The example neuron showed maximal response (solid purple line) to an OFF edge moving up. **E)** Leading edge receptive field (shaded cyan region), based on screen position of stimulus when thresholds were reached (dashed cyan lines). **F)** Screen position for grating (red), target (blue) and leading edge (cyan) receptive fields, for this example neuron. The data in panels A-D have been smoothed with a 100 ms square-wave filter and is shown at 40 kHz resolution.

Figure S4. Response to small bars is stronger in the dorsal, target receptive field. Response from a single example neuron to a bar of varying height traversing the entire width of the screen (mean ± SEM, n = 4) across either the target receptive field (blue) or the grating receptive field (red). The 50% contour lines and centres for the target receptive field (blue) and grating receptive field (red) for this neuron are shown. Grey shading indicates the analysis window used to calculate the mean response for this neuron in Figure 5A. Bar heights for each panel (A) 0.2°, (B) 0.8°, (C) 1.6°, (D) 3.1°, (E) 5.7°, (F) 11.2°, (G) 21.2°, (H) 39.7°, (I) 69.7°, (J) 106.5°, (K) 137.6°. The data have been smoothed with a 100 ms square-wave filter, and is shown at 40 kHz resolution.

Figure S5. Sensitivity to bar width depends on which receptive field it is in. Response from an example neuron to a bar of varying width traversing the entire height of the screen (mean ± SEM, n = 4). Pictograms indicate the position of the bar trajectory as it moved vertically up the screen (black dashed line and arrow), traversing first the grating receptive field (red) and then the target receptive field (blue). Shading indicates the two analysis windows used to calculate the mean neuronal response for this neuron in Figure 5B. Bar width for each panel (A) 0.2°, (B) 0.8°, (C) 1.6°, (D) 3.1°, (E) 5.7°, (F) 11.2°, (G) 21.2°, (H) 39.7°, (I) 69.7°, (J) 106.5°, (K) 137.6°, (L) 155.4°. The data have been smoothed with a 100 ms square-wave filter, and is shown at 40 kHz resolution.

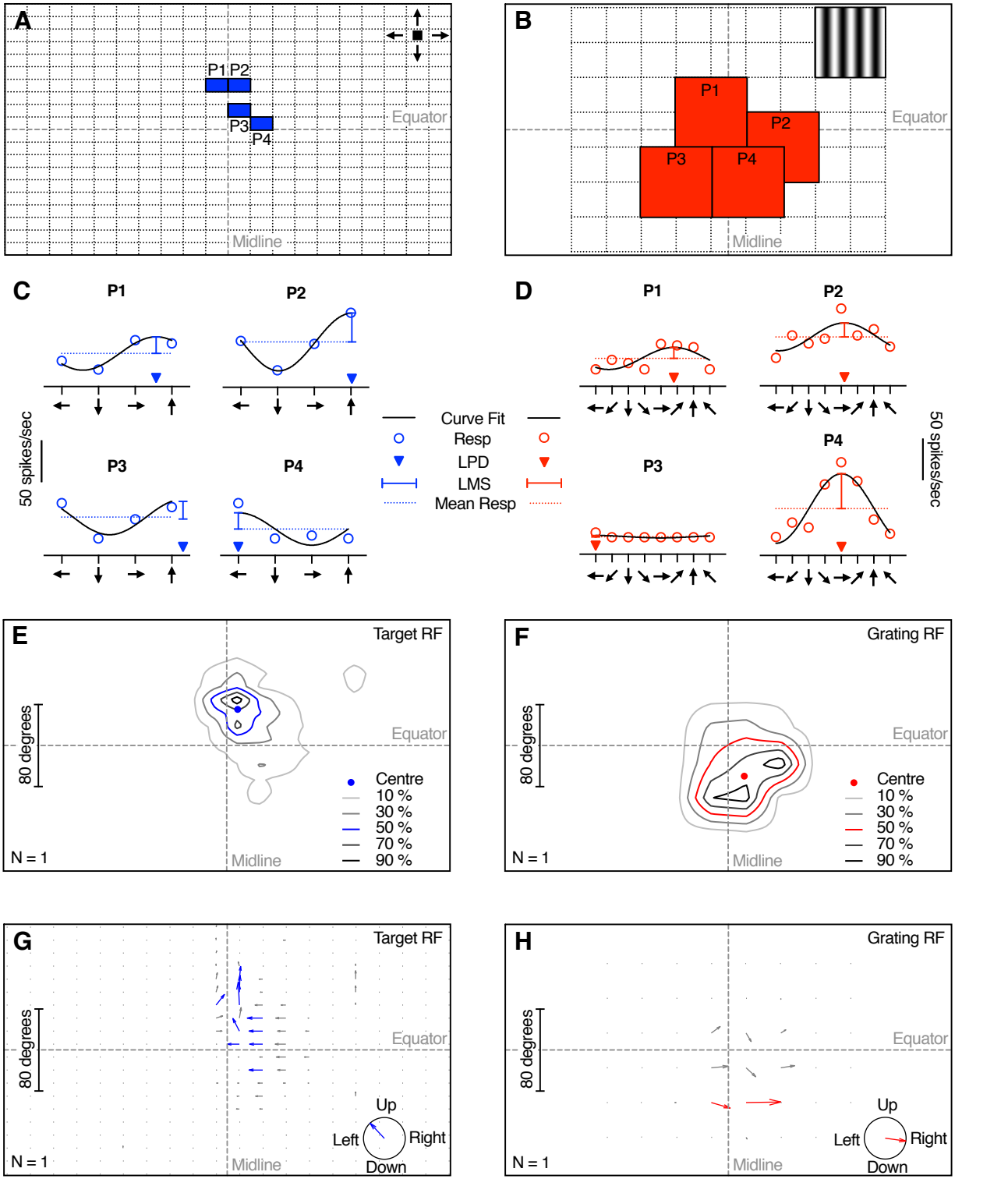
A
P1
P2
P3
P4
Equator
Midline
B
P1
P2
P3
P4
Equator
Midline
C
P1
P2
P3
P4
50 spikes/sec
Curve Fit
Resp
LPD
LMS
Mean Resp
D
P1
P2
P3
P4
50 spikes/sec
E
Target RF
80 degrees
Equator
Midline
N = 1
Centre
10 %
30 %
50 %
70 %
90 %
F
Grating RF
80 degrees
Equator
Midline
N = 1
Centre
10 %
30 %
50 %
70 %
90 %
G
Target RF
80 degrees
Equator
Midline
N = 1
Up
Left
Right
Down
H
Grating RF
80 degrees
Equator
Midline
N = 1
Up
Left
Right
Down

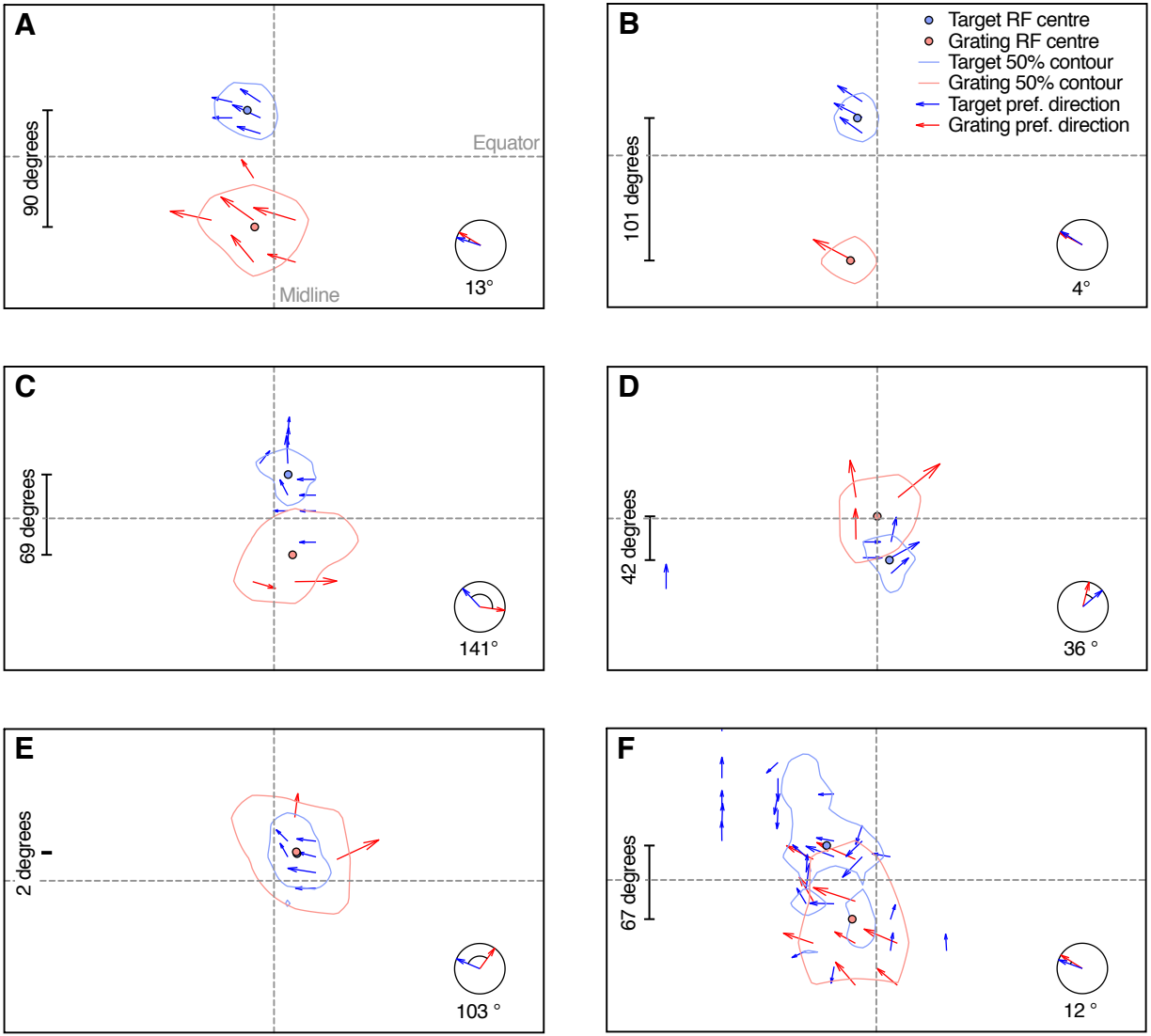
A
90 degrees
Equator
Midline
13°
B
101 degrees
4°
Target RF centre
Grating RF centre
Target 50% contour
Grating 50% contour
Target pref. direction
Grating pref. direction
C
69 degrees
141°
D
42 degrees
36 °
E
2 degrees
103 °
F
67 degrees
12 °

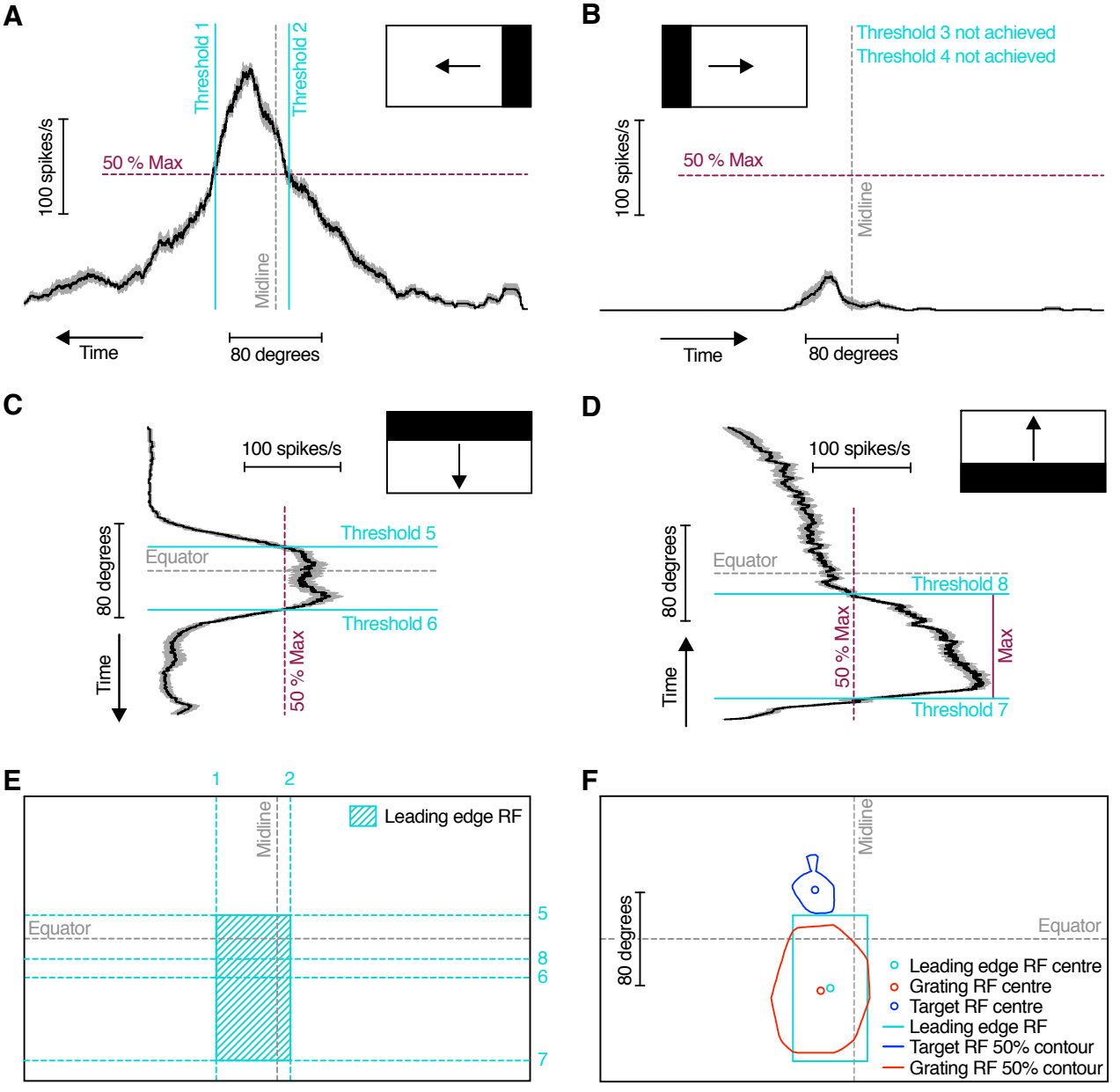
A
Threshold 1
Threshold 2
100 spikes/s
50 % Max
Midline
Time
80 degrees
B
Threshold 3 not achieved
Threshold 4 not achieved
100 spikes/s
50 % Max
Midline
Time
80 degrees
C
100 spikes/s
Threshold 5
Equator
80 degrees
Threshold 6
Time
50 % Max
D
100 spikes/s
Equator
Threshold 8
80 degrees
50 % Max
Max
Time
Threshold 7
E
1
2
Leading edge RF
Midline
Equator
5
8
6
7
F
Midline
80 degrees
Equator
Leading edge RF centre
Grating RF centre
Target RF centre
Leading edge RF
Target RF 50% contour
Grating RF 50% contour

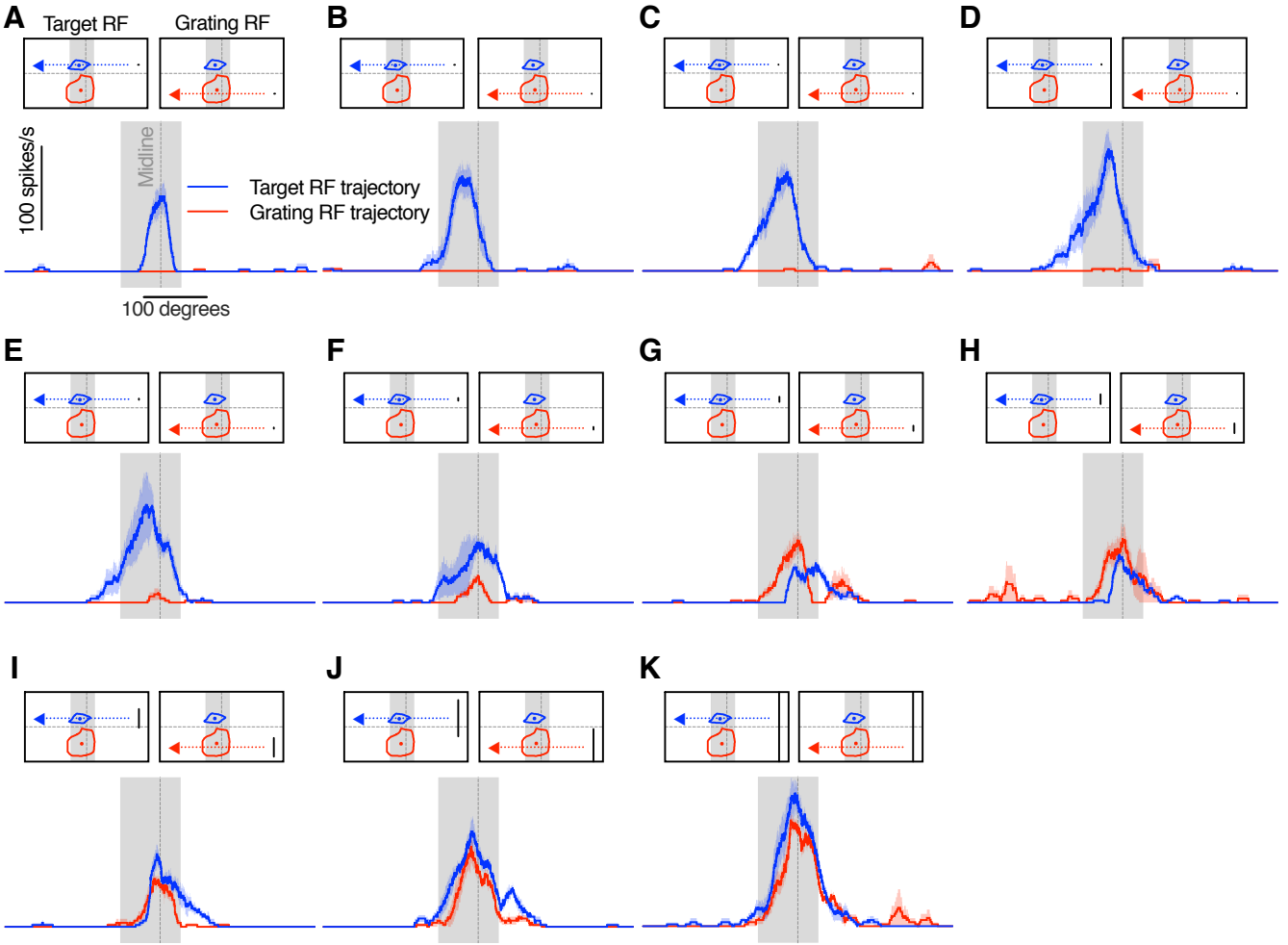
A
Target RF
Grating RF
B
C
D
100 spikes/s
Midline
Target RF trajectory
Grating RF trajectory
100 degrees
E
F
G
H
I
J
K

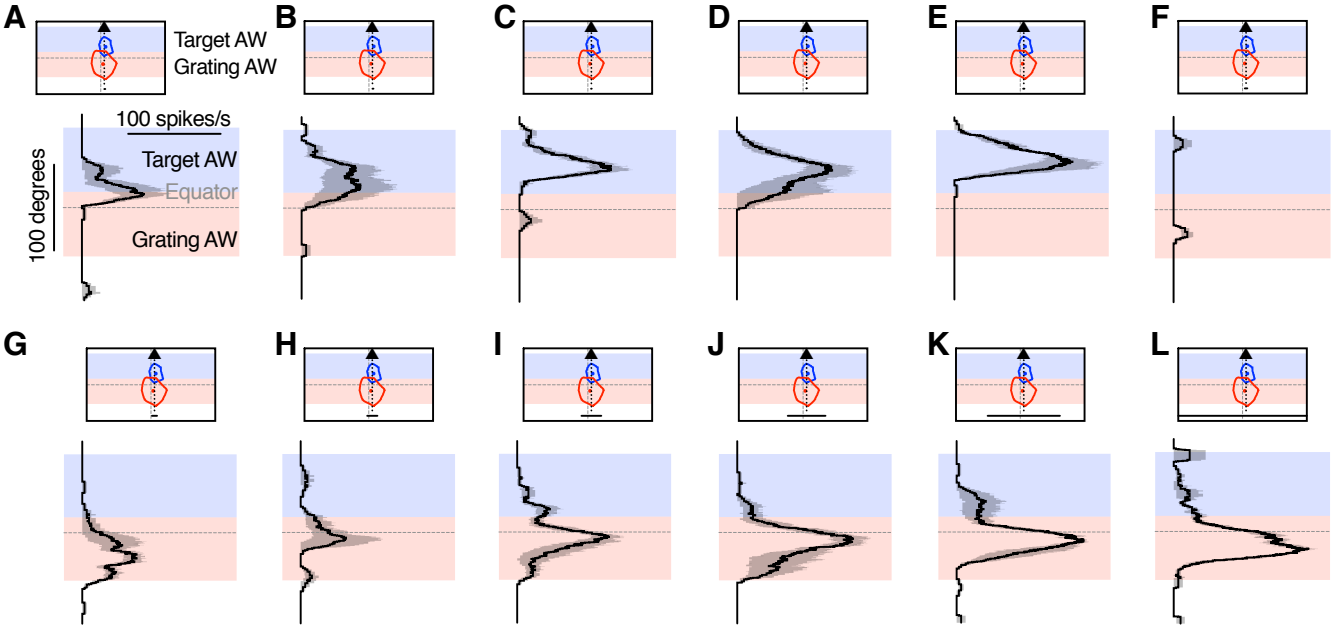
A
B
C
D
E
F
G
H
I
J
K
L
Target AW
Grating AW
100 spikes/s
Target AW
Equator
Grating AW
100 degrees